JACS
JOURNAL OF THE AMERICAN CHEMICAL SOCIETY
Article
pubs.acs.org/JACS

Olsalazine-Based Metal–Organic Frameworks as Biocompatible Platforms for H_2 Adsorption and Drug Delivery

Dana J. Levine,[†] Tomče Runčevski,[†,§] Matthew T. Kapelewski,[†,§] Benjamin K. Keitz,[†] Julia Oktawiec,[†] Douglas A. Reed,[†] Jarad A. Mason,[†,§] Henry Z. H. Jiang,[†,§] Kristen A. Colwell,[‡] Christina M. Legendre,[†] Stephen A. FitzGerald,[∥] and Jeffrey R. Long*[,†,‡,§]

[†]Department of Chemistry and [‡]Department of Chemical and Biomolecular Engineering, University of California, Berkeley, Berkeley, California 94720, United States

[§]Materials Sciences Division, Lawrence Berkeley National Laboratory, Berkeley, California 94720, United States

[∥]Department of Physics and Astronomy, Oberlin College, Oberlin, Ohio 44074, United States

Supporting Information

ABSTRACT: The drug olsalazine (H_4olz) was employed as a ligand to synthesize a new series of mesoporous metal–organic frameworks that are expanded analogues of the well-known M_2(dobdc) materials (dobdc^{4-} = 2,5-dioxido-1,4-benzenedicarboxylate; M-MOF-74). The M_2(olz) frameworks (M = Mg, Fe, Co, Ni, and Zn) exhibit high surface areas with large hexagonal pore apertures that are approximately 27 Å in diameter. Variable temperature H_2 adsorption isotherms revealed strong adsorption at the open metal sites, and *in situ* infrared spectroscopy experiments on Mg_2(olz) and Ni_2(olz) were used to determine site-specific H_2 binding enthalpies. In addition to its capabilities for gas sorption, the highly biocompatible Mg_2(olz) framework was also evaluated as a platform for the delivery of olsalazine and other encapsulated therapeutics. The Mg_2(olz) material (86 wt % olsalazine) was shown to release the therapeutic linker through dissolution of the framework under simulated physiological conditions. Furthermore, Mg_2(olz) was used to encapsulate phenethylamine (PEA), a model drug for a broad class of bioactive compounds. Under simulated physiological conditions, Mg_2(olz)$(PEA)_2$ disassembled to release PEA from the pores and olsalazine from the framework itself, demonstrating that multiple therapeutic components can be delivered together at different rates. The low toxicity, high surface areas, and coordinatively unsaturated metal sites make these M_2(olz) materials promising for a range of potential applications, including drug delivery in the treatment of gastrointestinal diseases.

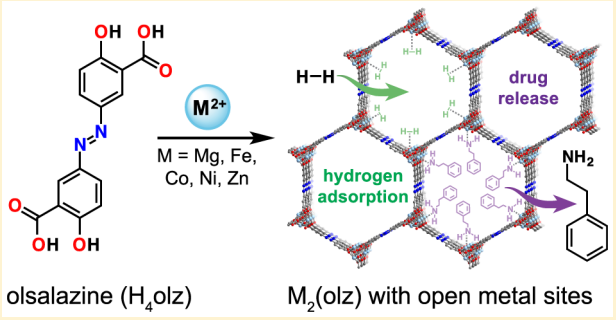

INTRODUCTION

Metal–organic frameworks (MOFs) are an important class of materials with high internal surface areas and tunable pore environments that make them of interest for a wide variety of potential applications, including gas adsorption,[1−4] catalysis,[5,6] conductivity,[7] and drug delivery.[8−10] One of the most ubiquitous materials in the literature is a series of isoreticular frameworks of the type M_2(dobdc) (2,5-dioxido-1,4-benzenedicarboxylate), sometimes referred to as M-MOF-74 or CPO-27-M. These frameworks are composed of dicationic metals and the tetraanionic linker dobdc^{4-} and feature one-dimensional hexagonal pores with open metal sites at the vertices.[11−15] The pores of these frameworks can be expanded while preserving the parent framework structure by using ligands such as 4,4′-dioxido-3,3′-biphenyldicarboxylate (dobpdc^{4-})[16] and other analogues with multiple phenylene groups.[17] Further variation can be introduced by using a structural isomer such as *m*-dobdc^{4-} (4,6-dioxido-1,3-benzenedicarboxylate), which alters the pore environment and enhances the positive charge densities of the open metal sites.[18] Notably, the Ni_2(*m*-dobdc) variant exhibits an H_2 binding enthalpy of −13.7 kJ/mol, which is the largest of any framework and −1.4 kJ/mol larger than the parent Ni_2(dobdc).

With an interest in exploring new ligands for expanded MOF-74 architectures, we sought to use the anti-inflammatory compound olsalazine, which exhibits the same coordinating functionality as dobpdc^{4-} while potentially having altered electronics.[19] Olsalazine is also slightly longer than dobpdc^{4-}, allowing it to accommodate larger guest molecules in the expanded pore of the corresponding framework. Olsalazine itself is a prodrug of the anti-inflammatory 5-aminosalicylic acid, and it is widely used in the treatment of ulcerative colitis and other gastrointestinal diseases.[20] Olsalazine has been shown to inhibit the development of colorectal cancer in patients,[21−23] and it has also been proposed as a broad spectrum anticancer agent.[24] Olsalazine is often taken daily in multigram doses,[25−27] making it an effectively nontoxic ligand that can be useful in the

Received: April 6, 2016
Published: August 3, 2016

ACS Publications © 2016 American Chemical Society

DOI: 10.1021/jacs.6b03523
J. Am. Chem. Soc. 2016, 138, 10143−10150

design of new materials. Indeed, there has been an increased focus on the development of low-toxicity metal−organic frameworks[28−34] due to the necessary safety and environmental considerations of their potential industrial applications.

Low-toxicity frameworks have also been explored as porous platforms for drug storage and release, and a broad spectrum of materials has been investigated for this purpose, including Cr-MIL-101,[35,36] the Fe-MIL series,[37−41] Zn-ZIF-8,[42−46] Zr-UiO derivatives,[47,48] and Fe_2(dobdc).[49,50] However, there are only a handful of metal−organic frameworks where a bioactive molecule serves as the sole bridging ligand. These materials include frameworks with iron and nicotinic acid (vitamin B_3),[51] zinc and the antibacterial azelaic acid,[52] hafnium and a photosensitizing porphyrin ligand for cancer therapy,[53] magnesium and the antioxidant gallic acid,[54] and zinc and the anti-inflammatory curcumin,[55] where the active organic component represents 59−79 wt % of the total framework. Of these, only a few materials have sufficiently large pores to encapsulate additional therapeutics. While several three-dimensional structures have also been reported with olsalazine as a bridging ligand,[56,57] they require ancillary or pillaring ligands that are not biocompatible, making them unsuitable materials for drug delivery applications.

In this study, a new family of expanded MOF-74 materials was synthesized using the anti-inflammatory olsalazine acid (H_4olz) as a ligand to form M_2(olz), where M = Mg, Fe, Co, Ni, and Zn. Upon activation, these materials exhibit the highest Langmuir surface areas among bioactive frameworks. The M_2(olz) frameworks contain pore apertures of approximately 27 Å, corresponding to the mesoporous range (≥20 Å). Strong H_2 adsorption was observed by gas adsorption studies and *in situ* infrared spectroscopy, confirming the presence of open metal sites for all but the Zn analogue. The Mg_2(olz) framework, which disassembles under physiological conditions to release olsalazine, represents an unprecedented level of loading in a bioactive metal−organic framework of 86 wt % drug. In addition to delivery of olsalazine, the large pores of Mg_2(olz) were used to encapsulate a second drug, illustrating the potential of this platform to deliver multiple therapeutic components. To this end, we demonstrated that the model drug phenethylamine (PEA) can be loaded into the pores of Mg_2(olz) to generate Mg_2(olz)$(PEA)_2$, and both PEA and olsalazine can be subsequently released under physiological conditions.

EXPERIMENTAL SECTION

All reagents and solvents were obtained from commercial sources at reagent-grade purity or higher. Synthesis of olsalazine (H_4olz) is described in the Supporting Information. Laboratory powder X-ray diffraction patterns were collected using Cu Kα radiation (λ = 1.5418 Å) on a Bruker AXS D8 Advance diffractometer equipped with a Göbel mirror and a Lynxeye linear position-sensitive detector and mounted with the following optics: a fixed divergence slit (0.6 mm), receiving slit (3 mm), and secondary-beam Soller slits (2.5°). The generator was set at 40 kV and 40 mA. Thermogravimetric analyses were carried out at a ramp rate of 2 °C/min under nitrogen flow with a TA Instruments Q5000. ^{1}H NMR experiments were carried out on a Bruker Avance III NMR spectrometer equipped with a BBO broadband probe operating at 600.13 MHz. Elemental analyses for C, H, and N were performed at the Microanalytical Laboratory of the University of California, Berkeley.

Synthesis of Mg_2(olz). The metal salt $Mg(NO_3)_2{\cdot}6H_2O$ (242 mg, 0.945 mmol) was dissolved in 12 mL of ethanol, and H_4olz (136 mg, 0.450 mmol) was dissolved separately in 18 mL of *N*,*N*-dimethylformamide (DMF). These solutions were combined in a 50 mL Pyrex glass jar, sealed, and heated in an isothermal oven at 120 °C for 1 day. The reaction mixture was subsequently decanted, and the damp yellow solid was washed with successive aliquots of DMF (3 × 30 mL) at 80 °C followed by aliquots of methanol (3 × 30 mL) at 60 °C. The slurry was then transferred to a tared analysis tube, and excess solvent was removed via cannula. The framework was activated for 12 h at 180 °C under a flow of argon and then placed under vacuum on an ASAP 2420 instrument at the same temperature. Activated yield: 125 mg (80% based on ligand). EA: calcd C 48.5%, H 1.70%, N 8.10%; found C 48.4%, H 1.55%, N 7.94%.

Synthesis of Fe_2(olz). In a nitrogen-filled glovebox, a 20 mL vial was charged with H_4olz (30 mg, 0.10 mmol) and $FeCl_2$ (30 mg, 0.24 mmol). Methanol (5 mL) and DMF (5 mL) were added, and the vial was sealed with a PTFE-lined cap and shaken until a homogeneous solution formed. The vial was placed on a dry bath preheated to 100 °C and left at this temperature, without stirring, for 16 h. The dark red/brown precipitate that had formed after this time was collected by filtration and washed with a small amount of methanol. The solid was washed with successive aliquots of DMF (3 × 15 mL) at 100 °C followed by aliquots of methanol (5 × 15 mL) at 60 °C. After the final wash, the dark red/brown solid was collected by filtration and dried under reduced pressure. In a glovebox, the methanol-solvated Fe_2(olz) was placed in a tared glass ASAP tube equipped with a Transeal. The tube was removed from the box and heated under vacuum to 120 °C at a rate of 0.2 °C/min to give Fe_2(olz). Activated yield: 26 mg (54% based on ligand). EA: calcd C 41.00%, H 1.50%, N 6.80%; found C 40.70%, H 1.18%, N 6.53%.

Synthesis of Co_2(olz). The metal salt $Co(NO_3)_2{\cdot}6H_2O$ (72.8 mg, 0.250 mmol) was dissolved in 3.3 mL of ethanol and 3.3 mL of water, and H_4olz (30.2 mg, 0.100 mmol) was dissolved separately in 3.3 mL of *N*,*N*-dimethylacetamide (DMA). The solutions were combined in a 10 mL Pyrex glass jar, sealed, and heated in an isothermal oven at 100 °C for 1 day. The reaction mixture was decanted, and the orange powder was washed with successive aliquots of DMF (3 × 10 mL) at 80 °C and methanol (3 × 10 mL) at 60 °C. The slurry was then transferred to a tared analysis tube where excess solvent was removed via cannula. The framework was activated for 12 h at 180 °C under an argon flow and then placed under vacuum at the same temperature on an ASAP 2420 instrument. Activated yield: 25.8 mg (62% based on ligand). EA: calcd C 40.40%, H 1.50%, N 6.70%; found C 40.13%, H 1.32%, N 6.84%.

Synthesis of Ni_2(olz). The metal salt $Ni(NO_3)_2{\cdot}6H_2O$ (218 mg, 0.750 mmol) was dissolved in 10 mL of ethanol and 10 mL of H_2O, and H_4olz (90.7 mg, 0.300 mmol) was dissolved separately in 10 mL of *N*,*N*-diethylformamide (DEF). These solutions were combined and then distributed into three 20 mL glass scintillation vials, sealed with a PTFE-lined cap, and heated in a dry bath at 100 °C for 1 day. The reaction mixtures were then combined, and the solvent was decanted. The resulting orange solid was washed with successive aliquots of DMF (3 × 20 mL) at 80 °C followed by aliquots of methanol (3 × 20 mL) at 60 °C. The slurry was then transferred to a tared analysis tube where excess solvent was removed via cannula. The framework was activated for 12 h at 180 °C under a flow of argon and then placed under vacuum at the same temperature on an ASAP 2420 instrument. Activated yield: 59.6 mg (62% based on ligand). EA: calcd C 40.50%, H 1.50%, N 6.70%; found C 40.58%, H 1.69%, N 6.53%.

Synthesis of Zn_2(olz). The metal salt $Zn(NO_3)_2{\cdot}6H_2O$ (298 mg, 1.00 mmol) was dissolved in 20 mL of ethanol, and H_4olz (121 mg, 0.400 mmol) was dissolved separately in 20 mL of DMA. These solutions were combined and then distributed into four 20 mL glass scintillation vials, sealed with a PTFE-lined cap, and heated in dry bath at 100 °C for 1 day. The reaction mixtures were then combined, and the solvent was decanted. The resulting yellow solid was washed with successive aliquots of DMF (3 × 20 mL) at 80 °C followed by aliquots of methanol (3 × 20 mL) at 60 °C. The resulting methanol slurry was then transferred to a tared analysis tube where excess solvent was removed. The framework was activated under argon flow at 100 °C for 12 h and then under vacuum at the same temperature on an ASAP 2420 instrument. Activated yield: 90.0 mg (52% based on ligand). EA:

DOI: 10.1021/jacs.6b03523
J. Am. Chem. Soc. 2016, 138, 10143−10150

calcd C 39.20%, H 1.40%, N 6.50%; found C 38.15%, H 1.34%, N 6.82%.

Preparation of Mg_2(olz)$(PEA)_2$. A 20% solution of phenethylamine in CH_2Cl_2 (500 μL) was sparged under N_2 and added to 6.5 mg of activated Mg_2(olz) in a vial under a nitrogen atmosphere, and the mixture was left undisturbed for 24 h. The product was then washed copiously with fresh CH_2Cl_2 and dried to obtain Mg_2(olz)$(PEA)_2$ as an orange-yellow solid (yield: 10.7 mg, 97%). Stoichiometry was confirmed by ^{1}H NMR spectroscopy upon digestion of the material in a 4% DCl solution in DMSO-d_6. An analogous procedure was also used to load *N*-methylphenethylamine into Mg_2(olz).

Gas Adsorption Measurements. Gas adsorption isotherms with pressures in the range 0−1.2 bar were measured using a volumetric method on either a Micromeritics ASAP 2020 or ASAP 2420 instrument. Samples were transferred under a N_2 or Ar atmosphere to tared analysis tubes and then capped with a Transeal. The samples were evacuated at the original activation temperature until the outgas rate was <1 μbar/min, at which point the tube was weighed to determine the mass of the activated sample. The tube was transferred to the analysis port of the instrument, and the outgas rate was again checked to ensure that it was below 1 μbar/min. UHP-grade (99.999% purity) N_2, H_2, and He were used for all adsorption measurements. For all isotherms, warm and cold free spaces were measured using He. N_2 and H_2 isotherms at 77 and 87 K were measured in liquid nitrogen and liquid argon baths, respectively. Oil-free vacuum pumps and oil-free pressure regulators were used for all measurements. Brunauer−Emmett−Teller (BET) surface areas were calculated from the linear region of the N_2 isotherms at 77 K prior to the step at 0.1 bar, and Langmuir surface areas were determined using Micromeritics software.

Powder X-ray Diffraction. Powder X-ray diffraction patterns of the samples were collected at the 17-BM beamline at the Advanced Photon Source (Argonne National Laboratory) with a wavelength of 0.72768 Å. Scattered intensity was recorded by PerkinElmer a-Si flat panel detector at room temperature. Prior to measurement, the samples were sealed under N_2 in borosilicate glass capillaries of 1 mm diameter. Powder diffraction data analyses (pattern indexing, profile fitting, Pawley refinement, and crystal structure model) were performed with the program TOPAS-Academic V4.125.[58] Specifically, a standard peak search followed by indexing via the single value decomposition approach allowed the determination of approximate unit cell dimensions. Precise unit cell dimensions were determined by performing a structureless Pawley refinement in TOPAS-Academic. A structural model was constructed in the refined unit cell by treating the olsalazine ligand as a rigid body and assuming the framework adopted the same structural connectivity as the M_2(dobpdc) frameworks.

Infrared Spectroscopy. Activated powder samples (~10 mg) were each loaded into a cup attached to a copper slab providing thermal contact to a coldfinger cryostat (Janis ST-300T), which was monitored by a Si-diode thermometer. The loading of each sample was performed under an atmosphere of Ar. The cup was then mounted in a custom-built sample chamber, which allowed DRIFTS experiments to be performed under a controlled atmosphere. A calibrated gas manifold was used to dose the sample chamber with known quantities of H_2 gas. IR spectra were acquired under different pressures of H_2 using a Bomem DA3Michelson interferometer equipped with a quartz-halogen source, CaF_2 beamsplitter, and a liquid nitrogen-cooled mercury−cadmium−telluride detector. A cutoff filter above 9000 cm^{-1} was used to prevent unwanted sample heating from the IR source.

Multicomponent Drug Release from Mg_2(olz)$(PEA)_2$. Pellets of Mg_2(olz)$(PEA)_2$ were prepared from a circular die with a 4 mm diameter and pressed in a vise for 15 min under a consistent pressure to produce 5.0 mg (±0.2 mg) pellets. Dissolution experiments were performed in triplicate, where the pellets were each placed in 50 mL conical tubes containing 25 mL of phosphate buffered saline (PBS). The tubes were oriented horizontally in a shaking incubator with bidimensional stirring at 60 rpm at 37 °C. Aliquots (100 μL) were collected at designated time points and filtered through a 0.45 μm filter. Samples were stored at room temperature prior to analysis. Release of phenethylamine and olsalazine was monitored by reversed-phase HPLC. The Agilent 1260 Infinity Series HPLC was equipped with a quaternary pump, diode array detector, and a Zorbax C18 column using a gradient of 50%−75% MeCN/H_2O (both with 0.05% trifluoroacetic acid) at 1 mL/min and a 30 μL sample injection volume. Solvents were filtered using a Millipore 0.2 μm nylon membrane. The peak area measured at full dissolution was normalized to 100% release of each drug and used to correlate observed peak intensity to percent release at each time point. Phenethylamine and olsalazine were monitored at 210 and 360 nm, respectively.

RESULTS AND DISCUSSION

Synthesis of M_2(olz). The M_2(olz) frameworks were synthesized via traditional solvothermal methods, and through optimization of reaction conditions such as solvent composition and temperature, it was possible to isolate microcrystalline powder samples for all investigated metals (Figure S1). Powder X-ray diffraction revealed that the solvated and activated M_2(olz) frameworks are all isostructural (Figure 1). The

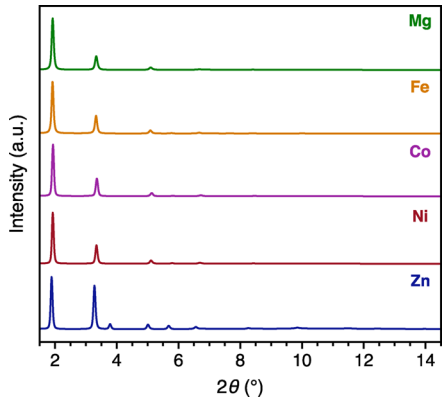

Figure 1. Powder X-ray diffraction patterns of activated M_2(olz) frameworks (M = Mg, Fe, Co, Ni) and ethanol-solvated Zn_2(olz); λ = 0.72768 Å. The diffraction patterns are offset for clarity.

diffraction patterns of M_2(olz) closely resemble those of M_2(dobdc) and M_2(dobpdc), suggesting a similar structure type (Figure S2). We therefore solved for the structure of M_2(olz) by assuming the same connectivity as these smaller analogues and refined our model against the collected diffraction patterns (Figure S3). A restrained Rietveld refinement was performed where the positions of the linker were frozen at the predicted fractional coordinates. The unit cell and profile parameters were then refined using the program TOPAS[58] and used to generate a structural model (Figure S4). Accordingly, we found that the M_2(olz) materials are isoreticular to the M_2(dobdc) frameworks and crystallize in the space group $P3_221$, exhibiting large pores that are approximately 27 Å wide. Unit cell parameters for each framework are given in Table S1, and their corresponding Pawley fits are shown in Figures S5−S9.

The as-synthesized M_2(olz) can be activated by performing successive solvent exchanges with DMF and methanol, followed by heating under argon and vacuum to remove residual or coordinated solvent. Surface areas of the desolvated M_2(olz) frameworks were then determined from N_2 adsorption measurements performed at 77 K (Figure S10). With the exception of Zn_2(olz), which loses crystallinity upon activation, the M_2(olz) frameworks exhibit high surface areas that are consistent with the expanded linker size (Table 1). The Langmuir surface areas are indeed the highest reported for any framework with a bioactive molecule as the sole linker.[55] In the

DOI: 10.1021/jacs.6b03523
J. Am. Chem. Soc. 2016, 138, 10143−10150

Table 1. Surface Areas of the M_2(olz) Frameworks

M	BET surface area (m^2/g)	Langmuir surface area (m^2/g)
Mg	2545	4593
Fe	1485	2618
Co	2060	3838
Ni	2067	3813
Zn	636	770

case of Mg_2(olz), Fe_2(olz), Co_2(olz), and Ni_2(olz), the N_2 adsorption isotherms exhibit a step at approximately 0.1 bar pressure. Similar behavior has been observed in the Ar adsorption isotherms of other frameworks in the expanded M_2(dobdc) series and is ascribed to the occupation of secondary adsorption sites.[17]

H_2 Adsorption in M_2(olz) Frameworks. In the isoreticular M_2(dobdc) series, the removal of axial metal-bound solvent molecules results in coordinatively unsaturated metal centers that are poised to interact with guest molecules such as CO_2,[59,60] NO,[50,61] and O_2.[15] These open metal sites are also particularly selective for H_2 adsorption,[62−64] and slight electronic changes afforded by replacing $dobdc^{4-}$ with *m*-$dobdc^{4-}$ further result in substantial enhancement of the H_2 binding enthalpies.[16] We therefore sought to confirm the presence of open metal sites within the structurally similar M_2(olz) frameworks and examine their potential as H_2 storage materials. Hydrogen adsorption isotherms were collected at 77 and 87 K for all activated M_2(olz) frameworks (Figure 2), and fits to the data were obtained employing the Langmuir−Freundlich equations for dual-site and trisite models (fit parameters are given in Table S2). Isosteric heats of adsorption (Q_{st}) were calculated using the Clausius−Clapeyron relation, which revealed strong H_2 binding at low coverage for the Mg, Fe, Co, and Ni frameworks, with Q_{st} values ranging from −10.8 to −12.1 kJ/mol (Figure 2 and Table 2). These values are comparable to those obtained for M_2(*m*-dobdc)[18] and M_2(dobpdc).[65]

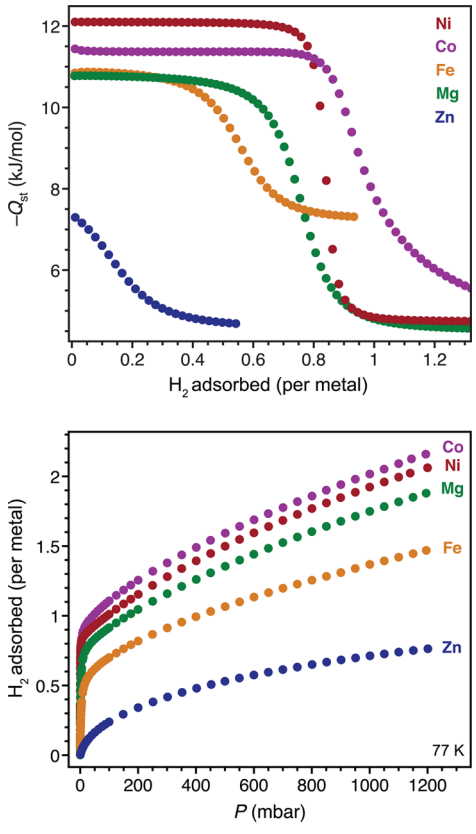

Figure 2. Top: isosteric heats of adsorption plotted as a function of the amount of H_2 adsorbed for M_2(olz). Bottom: equilibrium H_2 adsorption isotherms for M_2(olz) at 77 K, where the amount adsorbed is plotted in terms of H_2 molecules per metal atom.

Table 2. Isosteric Heats of Adsorption of H_2 in M_2(olz)

M	Mg	Fe	Co	Ni	Zn
Q_{st} (kJ/mol)	−10.8	−10.9	−11.4	−12.1	−7.3

As judged from the position of the inflection points in the isosteric heat plot of Figure 2 (upper), the performance of Co_2(olz) is notable because it shows near complete saturation of the metal centers. This high accessibility of the open metal sites is not observed in the smaller M_2(dobdc) or M_2(*m*-dobdc) materials, likely due to partially blocked pores. The Ni_2(olz) and Mg_2(olz) materials also exhibit reasonably good coverage at about 85% and 70% saturation, respectively. About 55% saturation is observed for Fe_2(olz), which may be due to the milder activation conditions employed for this material. In the case of Zn_2(olz), the isosteric heat of adsorption is significantly lower in magnitude than the other frameworks in the series. This material also does not exhibit a steep rise in H_2 adsorption at low pressures (Figure 2, lower), which suggests that open metal sites may not be present in the activated Zn_2(olz) material. This behavior is also consistent with the comparatively low surface area and loss in crystallinity observed upon activation.

Characterization of H_2−M_2(olz) Interactions by Infrared Spectroscopy. *In situ* infrared (IR) spectroscopy was used to further characterize the nature of the M_2(olz) interaction with H_2 for two of the highest performing materials, Mg_2(olz) and Ni_2(olz). Although H_2 is IR-inactive in the gas phase, its adsorption at surfaces breaks the vibrational symmetry, rendering the molecule IR-active (a schematic energy diagram is given in Figure S23). In particular, the binding of H_2 at open metal coordination sites with positive charge densities can be measured by a characteristic red-shift of the H−H stretching frequency. Importantly, recent studies have also shown that the magnitude of this frequency shift can be correlated to the strength of the binding energy at a particular site in the framework.[66] We examined the H_2 vibrational frequencies for Mg_2(olz) at several different loadings of H_2, as shown in Figure 3 (extended spectral ranges are given in Figure S24). At a loading of one H_2 per metal, a doublet is observed in the spectrum (maxima at 4097 and 4091 cm^{-1}) that corresponds to the pure vibrational modes of *ortho*-H_2 and *para*-H_2 bound to the open metal site. The spectrum of one H_2 bound to Ni_2(olz) exhibits a greater red-shift than that of H_2 bound to Mg_2(olz), which is consistent with stronger binding of H_2 to Ni^{2+} compared to Mg^{2+} in M_2(dobdc) (Figure S26). For both metals, the spectra indicate that the strength of H_2 binding is only slightly higher in the M_2(dobdc) than in M_2(olz) frameworks. Increasing the H_2 loading beyond 1 equiv per metal results in binding at secondary sites, as evidenced by the appearance of multiple peaks (from 4150 to 4100 cm^{-1}) in the IR spectra. Similar spectral features were observed for the secondary adsorption sites of M_2(dobdc) and M_2(*m*-dobdc) frameworks.[18] Additional increases in loading result in further

DOI: 10.1021/jacs.6b03523
J. Am. Chem. Soc. 2016, 138, 10143−10150

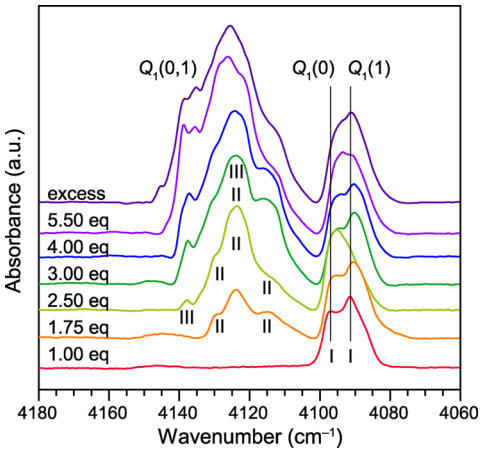

Figure 3. Hydrogen adsorbed at multiple sites as a function of loading. Infrared absorption of H_2 in Mg_2(olz) was performed at 15 K. The equivalents (eq) refer to the number of H_2 molecules per Mg, and the spectral features corresponding to the distinct sites observed are denoted with Roman numerals. $Q(0)$ refers to *para*-H_2 and $Q(1)$ to *ortho*-H_2 modes.

filling of the channels, giving rise to more complicated spectral features, indicating the presence of multiple binding sites within M_2(olz).

Variable-temperature IR spectra were also collected for Mg_2(olz) and Ni_2(olz) to extract the enthalpy of H_2 adsorption at the open metal sites (Figure 4).[67,68] The initial H_2 loading was set such that only the open metal sites were occupied during the measurements. The fractional occupancy was then determined as the ratio of the area under the resulting IR band to the area observed at complete saturation. The enthalpy and entropy changes were extracted from van't Hoff plots, which are shown as insets in Figure 4. We note that the slopes extracted from these plots are very sensitive to variation in the maximum saturation area, and an error of 1 kJ/mol can be estimated for the corresponding enthalpy values. For Ni_2(olz) the enthalpy of H_2 adsorption was found to be $\Delta H^\circ = -13(1)$ kJ/mol, which is higher than the $\Delta H^\circ = -10(1)$ kJ/mol of Mg_2(olz). Fairly large values of entropy changes were also measured for both frameworks ($\Delta S^\circ = -150(10)$ and $-130(10)$ J/K for Ni_2(olz) and Mg_2(olz), respectively), which is consistent with previous studies that revealed a positive correlation between the entropy and enthalpy change of bound H_2 in Mg_2(dobdc) and Co_2(dobdc).[68]

Mg_2(olz) as a Drug Delivery Platform. The high biocompatibility and large pore dimensions of the M_2(olz) frameworks make them promising candidates for drug delivery applications. Given the low atomic weight of Mg and its role as an essential metal in the human diet,[69] Mg_2(olz) was selected for the initial drug release studies. Notably, the desolvated material is composed of 86 wt % olsalazine, which represents one of the highest loadings for a therapeutic molecule in any reported metal−organic framework.[36,70] We prepared pellets of Mg_2(olz) framework and exposed them to simulated physiological conditions (37 °C PBS solution at pH 7.4 with bidimensional stirring at 60 rpm) to evaluate framework disassembly and olsalazine release. Aliquots were collected from the buffered solution at different time points, and the appearance of olsalazine was tracked by measuring its characteristic absorbance at 360 nm. The resulting degradation profile of Mg_2(olz) shows gradual release of olsalazine as the

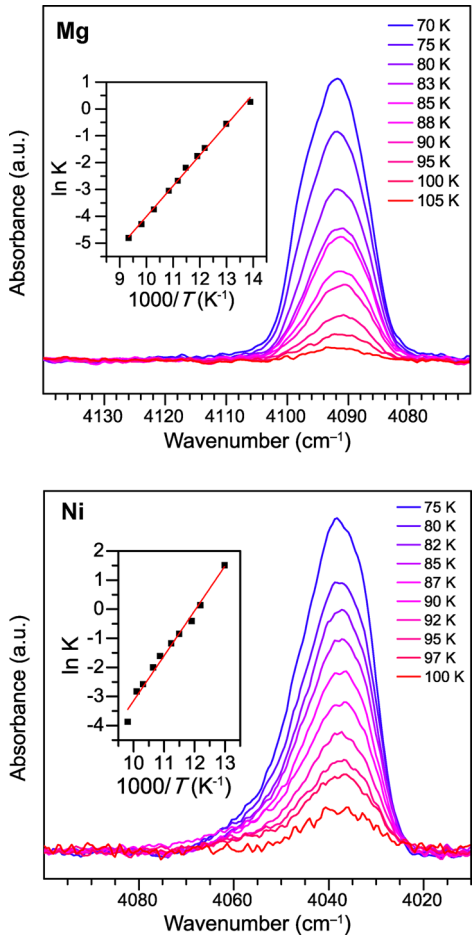

Figure 4. Enthalpy and entropy changes upon adsorption of H_2 on the open metal site. Variable-temperature infrared spectra were collected for Mg_2(olz) and Ni_2(olz), and the insets show the van't Hoff plots that were used to extract the enthalpy and entropy change in H_2 upon adsorption to the open metal site.

framework disassembles into its constituent parts (Figure S27). This release behavior, coupled with the high olsalazine composition, makes Mg_2(olz) a potential candidate for delivery of the anti-inflammatory therapeutic.

We further sought to utilize the high surface area and porosity of the Mg_2(olz) framework to codeliver a second drug with olsalazine. Phenethylamine (PEA) was selected as a model drug for loading because derivatives of this molecule form a large class of bioactive compounds with diverse pharmacological properties (e.g., stimulants, appetite suppressants, antidepressants, and anti-Parkinsonian agents; see Figure S28). Because of the extensive metabolism and addictive nature of some of these compounds, there is a need for controlled release formulations that reduce dramatic fluctuations in drug concentrations while maintaining adequate therapeutic levels over time. In this way, a controlled release dosage form may improve performance of the drug while reducing the likelihood of side effects and abuse.

Many approaches have been employed to load drugs into porous metal−organic frameworks including noncovalent drug encapsulation,[36,40,45,71,72] postsynthetic modification of the linker[39] or framework surface,[47] framework amorphization after loading,[48] "ship in a bottle",[73] and "bottle around ship"[43] strategies. An alternative approach is to use the drug as a ligand to bind to open metal sites within a framework, as has been

DOI: 10.1021/jacs.6b03523
J. Am. Chem. Soc. 2016, 138, 10143−10150

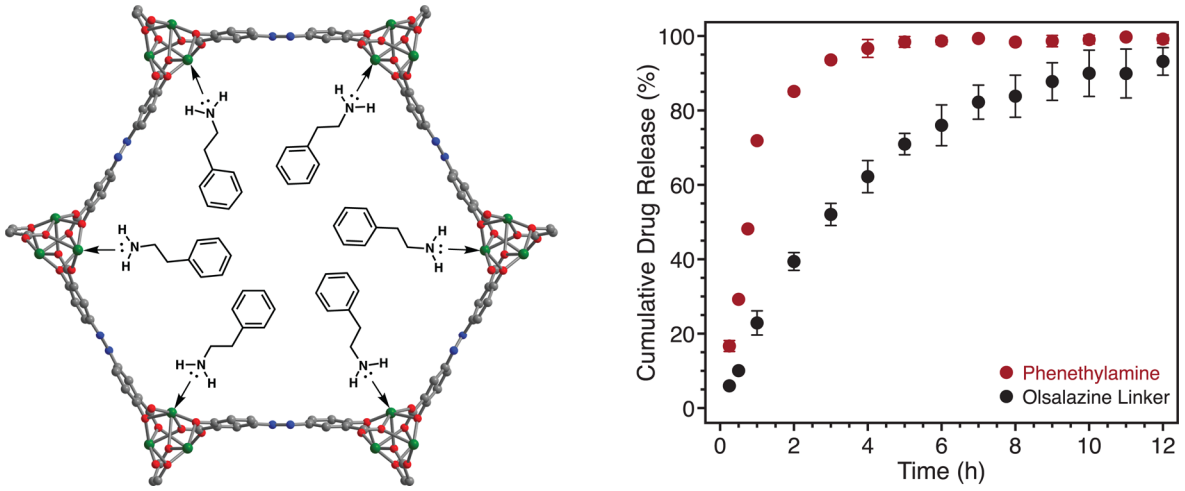

Figure 5. Left: proposed interaction of model drug phenethylamine with open metal sites of $Mg_2(olz)$. The framework structural model is from X-ray powder diffraction data, where green, red, blue, and gray spheres represent Mg, O, N, and C atoms, respectively; framework hydrogen atoms omitted for clarity. Right: release of phenethylamine and olsalazine from $Mg_2(olz)(PEA)_2$ under simulated biological conditions (PBS, pH = 7.4, 37 °C). Error bars represent standard deviation for release from triplicate pellet samples.

shown for anionic ibuprofen[49] and nitric oxide[50] in $Fe_2(dobdc)$. Taking advantage of the coordinatively unsaturated metal sites and large pore apertures of the $M_2(olz)$ frameworks, we sought to graft drugs containing a Lewis-basic functional group directly to the metal ions of the framework. Indeed, previous studies have demonstrated grafting of various functional groups, including amines,[16,74,75] alkoxides,[76] phenoxides,[77] and other anions[78] onto the open metal sites of $M_2(dobdc)$, $M_2(dobpdc)$, and MIL-101 frameworks. We therefore wanted to explore whether biologically active molecules possessing these functional groups could be similarly coordinated to the open metal sites of $Mg_2(olz)$.

To this end, PEA was incorporated into $Mg_2(olz)$ by soaking the framework in a 20% solution of the drug in CH_2Cl_2. After 24 h, the resulting material was washed and dried, and the stoichiometry was confirmed by ^1H NMR spectroscopy as two PEA per olsalazine, or one PEA per Mg^{2+} ion (Figure S29). A proposed structural model for $Mg_2(olz)(PEA)_2$ is depicted in Figure 5, where the amine of PEA is coordinated to the Mg^{2+} open metal sites in the observed 1:1 stoichiometry. The secondary amine *N*-methylphenethylamine was also shown to bind to $Mg_2(olz)$ in the expected stoichiometry of one amine per metal (Figure S30), suggesting that $Mg_2(olz)$ is a versatile platform that could accommodate a variety of phenethylamine derivatives or other small-molecule therapeutics.

In order to simulate physiological conditions for drug release, the $Mg_2(olz)(PEA)_2$ material was pressed into 4 mm pellets, which were immersed in PBS with shaking at 37 °C. Aliquots were taken at regular time points until the framework was fully dissolved, and release of both PEA and olsalazine was quantified by reversed-phase HPLC (Figure 5, right). Based on the observed cumulative release, the PEA is released more rapidly than the olsalazine linker. For example, approximately 95% of PEA was released compared to 50% of the olsalazine after 3 h. This result suggests that PEA may be displaced as water diffuses into the one-dimensional channels prior to the dissolution of the framework itself, resulting in multirate drug release.

In $Mg_2(olz)(PEA)_2$, over 90 wt % of the material consists of a therapeutic organic molecule, with PEA and olsalazine accounting for 41 and 51 wt %, respectively. Such high concentrations of active pharmaceutical ingredients are desirable as they can reduce the size of the administered dose and minimize the need for other components that may produce side effects in some patients. The disassembly of the loaded framework into components that have well-established pharmacological and safety profiles in humans is also a beneficial feature that may greatly expedite the translation of any promising $M_2(olz)$ materials into a clinical setting.

CONCLUSIONS

We have synthesized and characterized a new family of $M_2(olz)$ (M = Mg, Fe, Co, Ni, and Zn) metal−organic frameworks that utilize the anti-inflammatory drug olsalazine as the sole bridging ligand. The $M_2(olz)$ materials are the first series of isostructural bioactive frameworks exhibiting mesoporosity and can be made with a variety of metals. They contain 27 Å pores and have the highest Langmuir surface areas for metal−organic frameworks with a therapeutic linker. This level of mesoporosity can be useful in accommodating large guest molecules in the hexagonal channels. The $M_2(olz)$ materials are also the first bioactive metal−organic frameworks containing open metal sites, which may enhance interactions of encapsulated guest molecules within the pore. Indeed, these open metal sites have a strong affinity for binding H_2, as demonstrated by H_2 adsorption studies and *in situ* IR spectroscopy. While the volumetric capacity of $M_2(olz)$ frameworks may not be optimal for H_2 storage,[65] their high gravimetric capacity could be useful for other gas capture strategies that may benefit from an expanded pore size.

Notably, the $M_2(olz)$ frameworks have intrinsic therapeutic properties since they contain high quantities of the anti-inflammatory olsalazine, which can be released under simulated physiological conditions. This is especially true of $Mg_2(olz)$, the least dense $M_2(olz)$ framework, which represents the highest drug loading within any bioactive metal−organic framework to date. These mesoporous materials may also serve as platforms for the simultaneous delivery of multiple therapeutic compounds. This concept was demonstrated through the encapsulation of phenethylamine in $Mg_2(olz)$ and the successful release of both drugs under physiological conditions. The observed disassembly of the drug-loaded frameworks into

DOI: 10.1021/jacs.6b03523
J. Am. Chem. Soc. 2016, 138, 10143−10150

their original components is also advantageous for translation to clinical studies, since the safety and performance profiles will have been established previously for the constituent approved drugs.

Through judicious choice of metal, one can further envision tailoring the interaction between framework and drug to alter the strength of binding at the open metal site and tune the rate of release. For instance, the Mg_2(olz) and Co_2(olz) frameworks would be well suited for strong interactions with hard nitrogen and oxygen donors, while the Zn_2(olz) framework would be well matched for softer sulfur-based drugs loaded in solution. Additionally, the Fe_2(olz) framework could be oxidized to $[Fe_2(olz)]^{2+}$ as has been done for Fe_2(dobdc)[49] and Fe_2(dobpdc),[78] thereby producing a cationic framework capable of strong binding to anionic drugs. In some cases, it may also be beneficial to administer a precise ratio of metals in a drug formulation to serve as nutritional supplements or to address metal deficiencies in patients. Derivatives of M_2(dobdc) have been made with combinations of up to ten metals distributed throughout the framework in precise ratios,[79] and a similar strategy could be pursued with M_2(olz).

■ ASSOCIATED CONTENT

Supporting Information

The Supporting Information is available free of charge on the ACS Publications website at DOI: 10.1021/jacs.6b03523.

Synthesis of olsalazine, scanning electron microscopy, comparison of M_2(olz) to M_2(dobdc) and M_2(dobpdc), structural model of M_2(olz), Rietveld refinement, unit cell parameters and Pawley fits, 77 K N_2 adsorption isotherms, linear BET plots, thermogravimetric analysis, 77 and 87 K H_2 adsorption isotherms and fit parameters, IR spectra of H_2 binding to M_2(olz) and M_2(dobdc), release of olsalazine from Mg_2(olz) in PBS at 37 °C, examples of bioactive phenethylamine derivatives, NMR spectra of phenethylamine and *N*-methylphenethylamine loaded in Mg_2(olz), IR spectra of Mg_2(olz)$(PEA)_2$ and components (PDF)

■ AUTHOR INFORMATION

Corresponding Author

*E-mail: jrlong@berkeley.edu (J.R.L.).

Present Addresses

D.J.L.: Department of Chemical Engineering, California Institute of Technology, Pasadena, CA 91125.

B.K.K.: Department of Chemical Engineering, University of Texas at Austin, Austin, TX 78712.

J.A.M.: Department of Chemistry, Northwestern University, Evanston, IL 60208.

C.M.L.: Département de Chimie, École Normale Supérieure de Paris et Département de Chimie, Université Pierre et Marie Curie, 75005 Paris, France.

Notes

The authors declare no competing financial interest.

■ ACKNOWLEDGMENTS

This research was supported through the Department of Energy, Office of Energy Efficiency and Renewable Energy, Fuel Cell Technologies Office under Grant DE-AC02-05CH11231. We thank the 17-BM staff at the Advanced Photon Source at Argonne National Laboratory for assisting with powder X-ray diffraction experiments. Use of the Advanced Photon Source at Argonne National Laboratory was supported by the U.S. Department of Energy, Office of Science, Office of Basic Energy Sciences, under Contract DE-AC02-06CH11357. We gratefully acknowledge the NDSEG for providing fellowship support for D.J.L. and the NSF for supporting M.T.K., J.O., D.A.R., and J.A.M. We also thank M. I. Gonzalez for helpful discussions and Dr. K. R. Meihaus for editorial assistance.

■ REFERENCES

(1) Sumida, K.; Rogow, D. L.; Mason, J. A.; McDonald, T. M.; Bloch, E. D.; Herm, Z. R.; Bae, T.-H.; Long, J. R. *Chem. Rev.* **2012**, *112* (2), 724.

(2) Suh, M. P.; Park, H. J.; Prasad, T. K.; Lim, D.-W. *Chem. Rev.* **2012**, *112* (2), 782.

(3) He, Y.; Zhou, W.; Qian, G.; Chen, B. *Chem. Soc. Rev.* **2014**, *43* (16), 5657.

(4) Barea, E.; Montoro, C.; Navarro, J. *Chem. Soc. Rev.* **2014**, *43* (16), 5419.

(5) Corma, A.; Garcia, H.; Llabrés i Xamena, F. X. *Chem. Rev.* **2010**, *110* (8), 4606.

(6) Chughtai, A. H.; Ahmad, N.; Younus, H. A.; Laypkov, A.; Verpoort, F. *Chem. Soc. Rev.* **2015**, *44* (19), 6804.

(7) Sun, L.; Campbell, M. G.; Dincă, M. *Angew. Chem., Int. Ed.* **2016**, *55* (11), 3566.

(8) Della Rocca, J.; Liu, D.; Lin, W. *Acc. Chem. Res.* **2011**, *44* (10), 957.

(9) Horcajada, P.; Gref, R.; Baati, T.; Maurin, G.; Couvreur, P.; Férey, G.; Morris, R. E.; Serre, C. *Chem. Rev.* **2012**, *112* (2), 1232.

(10) Sun, C.-Y.; Qin, C.; Wang, X.-L.; Su, Z.-M. *Expert Opin. Drug Delivery* **2013**, *10* (1), 89.

(11) Dietzel, P. D. C.; Morita, Y.; Blom, R.; Fjellvåg, H. *Angew. Chem.* **2005**, *117* (39), 6512.

(12) Rosi, N. L.; Kim, J.; Eddaoudi, M.; Chen, B.; O'Keeffe, M.; Yaghi, O. M. *J. Am. Chem. Soc.* **2005**, *127* (5), 1504.

(13) Dietzel, P. D. C.; Panella, B.; Hirscher, M.; Blom, R.; Fjellvåg, H. *Chem. Commun.* **2006**, *0* (9), 959.

(14) Caskey, S. R.; Wong-Foy, A. G.; Matzger, A. J. *J. Am. Chem. Soc.* **2008**, *130* (33), 10870.

(15) Bloch, E. D.; Murray, L. J.; Queen, W. L.; Chavan, S.; Maximoff, S. N.; Bigi, J. P.; Krishna, R.; Peterson, V. K.; Grandjean, F.; Long, G. J.; Smit, B.; Bordiga, S.; Brown, C. M.; Long, J. R. *J. Am. Chem. Soc.* **2011**, *133* (37), 14814.

(16) McDonald, T. M.; Lee, W. R.; Mason, J. A.; Wiers, B. M.; Hong, C. S.; Long, J. R. *J. Am. Chem. Soc.* **2012**, *134* (16), 7056.

(17) Deng, H.; Grunder, S.; Cordova, K. E.; Valente, C.; Furukawa, H.; Hmadeh, M.; Gándara, F.; Whalley, A. C.; Liu, Z.; Asahina, S.; Kazumori, H.; O'Keeffe, M.; Terasaki, O.; Stoddart, J. F.; Yaghi, O. M. *Science* **2012**, *336* (6084), 1018.

(18) Kapelewski, M. T.; Geier, S. J.; Hudson, M. R.; Stück, D.; Mason, J. A.; Nelson, J. N.; Xiao, D. J.; Hulvey, Z.; Gilmour, E.; FitzGerald, S. A.; Head-Gordon, M.; Brown, C. M.; Long, J. R. *J. Am. Chem. Soc.* **2014**, *136* (34), 12119.

(19) Eriksson, A.; Nyholm, L. *Electrochim. Acta* **2001**, *46*, 1113.

(20) Selby, W. S.; Barr, G. D.; Ireland, A.; Mason, C. H.; Jewell, D. P. *Br. Med. J. (Clin. Res. Ed.)* **1985**, *291* (6506), 1373.

(21) Brown, W. A.; Farmer, K. C.; Skinner, S. A.; Malcontenti-Wilson, C.; Misajon, A.; O'Brien, P. E. *Dig. Dis. Sci.* **2000**, *45* (8), 1578.

(22) Eaden, J. *Aliment. Pharmacol. Ther.* **2003**, *18* (S2), 15.

(23) Herfarth, H. *Dig. Dis.* **2012**, *30* (Suppl. 2), 55.

(24) Méndez-Lucio, O.; Tran, J.; Medina-Franco, J. L.; Meurice, N.; Muller, M. *ChemMedChem.* **2014**, *9* (3), 560.

(25) Campbell, D. E. S.; Berglindh, T. *Scand. J. Gastroenterol.* **1988**, *23* (s148), 7.

(26) Courtney, M. G.; Nunes, D. P.; Bergin, C. F.; O'Driscoll, M.; Trimble, V.; Keeling, P. W.; Weir, D. G. *Lancet* **1992**, *339* (8804), 1279.

DOI: 10.1021/jacs.6b03523
J. Am. Chem. Soc. 2016, 138, 10143−10150

(27) Kles, K. A.; Vavricka, S. R.; Turner, J. R.; Musch, M. W.; Hanauer, S. B.; Chang, E. B. *Inflamm. Bowel Dis.* **2005**, *11* (3), 253.
(28) Smaldone, R. A.; Forgan, R. S.; Furukawa, H.; Gassensmith, J. J.; Slawin, A. M. Z.; Yaghi, O. M.; Stoddart, J. F. *Angew. Chem., Int. Ed.* **2010**, *49* (46), 8630.
(29) An, J.; Farha, O. K.; Hupp, J. T.; Pohl, E.; Yeh, J. I.; Rosi, N. L. *Nat. Commun.* **2012**, *3*, 604.
(30) Li, T.; Chen, D.-L.; Sullivan, J. E.; Kozlowski, M. T.; Johnson, J. K.; Rosi, N. L. *Chem. Sci.* **2013**, *4* (4), 1746.
(31) Miller, S. R.; Alvarez, E.; Fradcourt, L.; Devic, T.; Wuttke, S.; Wheatley, P. S.; Steunou, N.; Bonhomme, C.; Gervais, C.; Laurencin, D.; Morris, R. E.; Vimont, A.; Daturi, M.; Horcajada, P.; Serre, C. *Chem. Commun.* **2013**, *49* (71), 7773.
(32) Baati, T.; Njim, L.; Neffati, F.; Kerkeni, A.; Bouttemi, M.; Gref, R.; Najjar, M. F.; Zakhama, A.; Couvreur, P.; Serre, C.; Horcajada, P. *Chem. Sci.* **2013**, *4* (4), 1597.
(33) Kathalikkattil, A. C.; Babu, R.; Roshan, R. K.; Lee, H.; Kim, H.; Tharun, J.; Suresh, E.; Park, D.-W. *J. Mater. Chem. A* **2015**, *3* (45), 22636.
(34) Noro, S.-I.; Mizutani, J.; Hijikata, Y.; Matsuda, R.; Sato, H.; Kitagawa, S.; Sugimoto, K.; Inubushi, Y.; Kubo, K.; Nakamura, T. *Nat. Commun.* **2015**, *6*, 5851.
(35) Férey, G.; Mellot-Draznieks, C.; Serre, C.; Millange, F.; Dutour, J.; Surblé, S.; Margiolaki, I. *Science* **2005**, *309* (5743), 2040.
(36) Horcajada, P.; Serre, C.; Vallet-Regí, M.; Sebban, M.; Taulelle, F.; Férey, G. *Angew. Chem.* **2006**, *118* (36), 6120.
(37) Horcajada, P.; Surblé, S.; Serre, C.; Hong, D.-Y.; Seo, Y.-K.; Chang, J.-S.; Grenèche, J.-M.; Margiolaki, I.; Férey, G. *Chem. Commun.* **2007**, No. 27, 2820.
(38) Horcajada, P.; Serre, C.; Maurin, G.; Ramsahye, N. A.; Balas, F.; Vallet-Regí, M.; Sebban, M.; Taulelle, F.; Férey, G. *J. Am. Chem. Soc.* **2008**, *130* (21), 6774.
(39) Taylor-Pashow, K. M. L.; Rocca; Della, J.; Xie, Z.; Tran, S.; Lin, W. *J. Am. Chem. Soc.* **2009**, *131* (40), 14261.
(40) Horcajada, P.; Chalati, T.; Serre, C.; Gillet, B.; Sebrie, C.; Baati, T.; Eubank, J. F.; Heurtaux, D.; Clayette, P.; Kreuz, C.; Chang, J.-S.; Hwang, Y. K.; Marsaud, V.; Bories, P.-N.; Cynober, L.; Gil, S.; Férey, G.; Couvreur, P.; Gref, R. *Nat. Mater.* **2010**, *9* (2), 172.
(41) Chalati, T.; Horcajada, P.; Couvreur, P.; Serre, C.; Ben Yahia, M.; Maurin, G.; Gref, R. *Nanomedicine* **2011**, *6* (10), 1683.
(42) Vasconcelos, I. B.; Silva, T. G. D.; Militão, G. C. G.; Soares, T. A.; Rodrigues, N. M.; Rodrigues, M. O.; Costa, N. B. D.; Freire, R. O.; Junior, S. A. *RSC Adv.* **2012**, *2* (25), 9437.
(43) Liédana, N.; Galve, A.; Rubio, C.; Téllez, C.; Coronas, J. *ACS Appl. Mater. Interfaces* **2012**, *4* (9), 5016.
(44) Wu, Y. N.; Zhou, M.; Li, S.; Li, Z.; Li, J.; Wu, B.; Li, G.; Li, F.; Guan, X. *Small* **2014**, *10* (14), 2927.
(45) Zhuang, J.; Kuo, C.-H.; Chou, L.-Y.; Liu, D.-Y.; Weerapana, E.; Tsung, C.-K. *ACS Nano* **2014**, *8* (3), 2812.
(46) Zheng, H.; Zhang, Y.; Liu, L.; Wan, W.; Guo, P.; Nyström, A. M.; Zou, X. *J. Am. Chem. Soc.* **2016**, *138* (3), 962.
(47) He, C.; Lu, K.; Liu, D.; Lin, W. *J. Am. Chem. Soc.* **2014**, *136* (14), 5181.
(48) Orellana-Tavra, C.; Baxter, E. F.; Tian, T.; Bennett, T. D.; Slater, N. K. H.; Cheetham, A. K.; Fairen-Jimenez, D. *Chem. Commun.* **2015**, *51* (73), 13878.
(49) Hu, Q.; Yu, J.; Liu, M.; Liu, A.; Dou, Z.; Yang, Y. *J. Med. Chem.* **2014**, *57* (13), 5679.
(50) Bloch, E. D.; Queen, W. L.; Chavan, S.; Wheatley, P. S.; Zadrozny, J. M.; Morris, R.; Brown, C. M.; Lamberti, C.; Bordiga, S.; Long, J. R. *J. Am. Chem. Soc.* **2015**, *137* (10), 3466.
(51) Miller, S. R.; Heurtaux, D.; Baati, T.; Horcajada, P.; Grenèche, J.-M.; Serre, C. *Chem. Commun.* **2010**, *46* (25), 4526.
(52) Tamames-Tabar, C.; Imbuluzqueta, E.; Guillou, N.; Serre, C.; Miller, S. R.; Elkaim, E.; Horcajada, P.; Blanco-Prieto, M. J. *CrystEngComm* **2015**, *17* (2), 456.
(53) Lu, K.; He, C.; Lin, W. *J. Am. Chem. Soc.* **2014**, *136* (48), 16712.
(54) Cooper, L.; Hidalgo, T.; Gorman, M.; Lozano-Fernández, T.; Simón-Vázquez, R.; Olivier, C.; Guillou, N.; Serre, C.; Martineau, C.; Taulelle, F.; Damasceno-Borges, D.; Maurin, G.; González-Fernández, Á.; Horcajada, P.; Devic, T. *Chem. Commun.* **2015**, *51* (27), 5848.
(55) Su, H.; Sun, F.; Jia, J.; He, H.; Wang, A.; Zhu, G. *Chem. Commun.* **2015**, *51*, 5774.
(56) Xiao, D.-R.; Sun, D.-Z.; Liu, J.-L.; Zhang, G.-J.; Chen, H.-Y.; He, J.-H.; Yan, S.-W.; Yuan, R.; Wang, E.-B. *Eur. J. Inorg. Chem.* **2011**, *2011* (24), 4656.
(57) Chen, H.-Y.; Xiao, D.-R.; Yan, S.-W.; He, J.-H.; Yang, J.; Wang, X.; Yuan, R.; Wang, E.-B. *Inorg. Chim. Acta* **2012**, *387* (C), 283.
(58) TOPAS Academic, Bruker AXS. V.4.125, 2007.
(59) Britt, D.; Furukawa, H.; Wang, B.; Glover, T. G.; Yaghi, O. M. *Proc. Natl. Acad. Sci. U. S. A.* **2009**, *106* (49), 20637.
(60) Queen, W. L.; Hudson, M. R.; Bloch, E. D.; Mason, J. A.; Gonzalez, M. I.; Lee, J. S.; Gygi, D.; Howe, J. D.; Lee, K.; Darwish, T. A.; James, M.; Peterson, V. K.; Teat, S. J.; Smit, B.; Neaton, J. B.; Long, J. R.; Brown, C. M. *Chem. Sci.* **2014**, *5* (12), 4569.
(61) McKinlay, A. C.; Xiao, B.; Wragg, D. S.; Wheatley, P. S.; Megson, I. L.; Morris, R. E. *J. Am. Chem. Soc.* **2008**, *130* (31), 10440.
(62) Dietzel, P. D. C.; Georgiev, P. A.; Eckert, J.; Blom, R.; Strässle, T.; Unruh, T. *Chem. Commun.* **2010**, *46* (27), 4962.
(63) Sumida, K.; Brown, C. M.; Herm, Z. R.; Chavan, S.; Bordiga, S.; Long, J. R. *Chem. Commun.* **2011**, *47* (4), 1157.
(64) Queen, W. L.; Bloch, E. D.; Brown, C. M.; Hudson, M. R.; Mason, J. A.; Murray, L. J.; Ramirez-Cuesta, A. J.; Peterson, V. K.; Long, J. R. *Dalton Trans.* **2012**, *41* (14), 4180.
(65) Gygi, D.; Bloch, E. D.; Mason, J. A.; Hudson, M. R.; Gonzalez, M. I.; Siegelman, R. L.; Darwish, T. A.; Queen, W. L.; Brown, C. M.; Long, J. R. *Chem. Mater.* **2016**, *28* (4), 1128.
(66) FitzGerald, S. A.; Burkholder, B.; Friedman, M.; Hopkins, J. B.; Pierce, C. J.; Schloss, J. M.; Thompson, B.; Rowsell, J. L. C. *J. Am. Chem. Soc.* **2011**, *133* (50), 20310.
(67) Garrone, E.; Bonelli, B.; Otero Areán, C. *Chem. Phys. Lett.* **2008**, *456* (1−3), 68.
(68) Areán, C. O.; Chavan, S.; Cabello, C. P.; Garrone, E.; Palomino, G. T. *ChemPhysChem* **2010**, *11* (15), 3237.
(69) Vormann, J. *Mol. Aspects Med.* **2003**, *24*, 27.
(70) He, C.; Liu, D.; Lin, W. *Chem. Rev.* **2015**, *115* (19), 11079.
(71) Wang, H.-N.; Meng, X.; Yang, G.-S.; Wang, X.-L.; Shao, K.-Z.; Su, Z.-M.; Wang, C.-G. *Chem. Commun.* **2011**, *47* (25), 7128.
(72) Sun, C.-Y.; Qin, C.; Wang, C.-G.; Su, Z.-M.; Wang, S.; Wang, X.-L.; Yang, G.-S.; Shao, K.-Z.; Lan, Y.-Q.; Wang, E.-B. *Adv. Mater.* **2011**, *23* (47), 5629.
(73) di Nunzio, M. R.; Agostoni, V.; Cohen, B.; Gref, R.; Douhal, A. *J. Med. Chem.* **2014**, *57* (2), 411.
(74) McDonald, T. M.; Mason, J. A.; Kong, X.; Bloch, E. D.; Gygi, D.; Dani, A.; Crocellà, V.; Giordanino, F.; Odoh, S. O.; Drisdell, W. S.; Vlaisavljevich, B.; Dzubak, A. L.; Poloni, R.; Schnell, S. K.; Planas, N.; Lee, K.; Pascal, T.; Wan, L. F.; Prendergast, D.; Neaton, J. B.; Smit, B.; Kortright, J. B.; Gagliardi, L.; Bordiga, S.; Reimer, J. A.; Long, J. R. *Nature* **2015**, *519* (7543), 303.
(75) Nguyen, H. G. T.; Weston, M. H.; Farha, O. K.; Hupp, J. T.; Nguyen, S. T. *CrystEngComm* **2012**, *14* (12), 4115.
(76) Wiers, B. M.; Foo, M.-L.; Balsara, N. P.; Long, J. R. *J. Am. Chem. Soc.* **2011**, *133* (37), 14522.
(77) Aubrey, M. L.; Ameloot, R.; Wiers, B. M.; Long, J. R. *Energy Environ. Sci.* **2014**, *7* (2), 667.
(78) Aubrey, M. L.; Long, J. R. *J. Am. Chem. Soc.* **2015**, *137* (42), 13594.
(79) Wang, L. J.; Deng, H.; Furukawa, H.; Gándara, F.; Cordova, K. E.; Peri, D.; Yaghi, O. M. *Inorg. Chem.* **2014**, *53* (12), 5881.

DOI: 10.1021/jacs.6b03523
J. Am. Chem. Soc. 2016, 138, 10143−10150